

SEED: Towards More Accurate Semantic Evaluation for Visual Brain Decoding

Juhyeon Park^{1*}, Peter Yongho Kim^{2*}, Jiook Cha³, Shinjae Yoo⁴, and Taesup Moon^{1, 2, 5†}

{parkjh9229, peterkim98, connectome, tsmoon}@snu.ac.kr, sjyoo@bnl.gov

¹ IPAI, Seoul National University ² ECE, Seoul National University

³ Psychology, Seoul National University

⁴ Brookhaven National Lab

⁵ ASRI / INMC / AIIS, Seoul National University

Abstract

We present *SEED* (*Semantic Evaluation for Visual Brain Decoding*), a novel metric for evaluating the semantic decoding performance of visual brain decoding models. It integrates three complementary metrics, each capturing a different aspect of semantic similarity between images. Using carefully crowd-sourced human judgment data, we demonstrate that *SEED* achieves the highest alignment with human evaluations, outperforming other widely used metrics. Through the evaluation of existing visual brain decoding models, we further reveal that crucial information is often lost in translation, even in state-of-the-art models that achieve near-perfect scores on existing metrics. To facilitate further research, we open-source the human judgment data, encouraging the development of more advanced evaluation methods for brain decoding models. Additionally, we propose a novel loss function designed to enhance semantic decoding performance by leveraging the order of pairwise cosine similarity in CLIP image embeddings. This loss function is compatible with various existing methods and has been shown to consistently improve their semantic decoding performances when used for training, with respect to both existing metrics and *SEED*.

1. Introduction

Visual brain decoding focuses on reconstructing visual stimuli from brain signals, such as functional magnetic resonance imaging (fMRI), thereby bridging the fields of neuroscience and computer vision. This field of research is pivotal for developing brain-computer interface (BCI) systems [7, 19, 28, 43] and provides key insights into the working mechanisms of complex human perceptual systems [19].

*Equal contribution. The order of the co-first authors was determined by a coin toss.

†Corresponding author

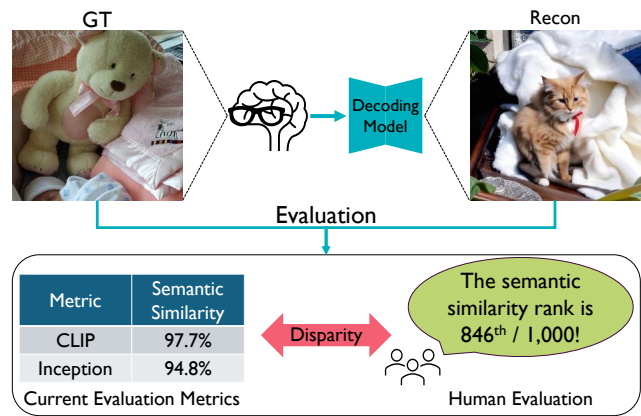


Figure 1. Current evaluation metrics assess the semantic similarity between ground-truth and reconstructions in a way that significantly differs from human judgment, often giving relatively high scores to reconstructions that are semantically misaligned.

Reflecting its importance, numerous studies have been dedicated to advancing this domain [4, 11, 15, 29, 30, 36, 38, 39, 42].

With the recent advent of diffusion-based decoding models [11, 29, 30, 36, 38] that boast a near-perfect performance on all of the percentage-based evaluation metrics, the endeavor to visually decode brain signals might seem to be nearly solved, with little to no room for improvement for future research. However, upon close inspection, the decoding results, even from the most recent and state-of-the-art models, often seem to fail at reconstructing crucial semantic elements in the original image; *e.g.*, a teddy bear may turn into a cat during the reconstruction process. (See Fig. 1)

As this example suggests, we observed that current evaluation metrics tend to assign relatively high scores to such flawed reconstructions, potentially misleading researchers and obscuring the true limitations of these models. This leads to the following question: *Is the current framework to evaluate visual decoding models sufficient?* To answer that,

we first inspected current evaluation metrics and identified a few limitations: the dependency on the comparison image pool, insufficient difficulty, and the lack of human-likeness. Furthermore, metrics used in related domains, such as FID or SSIM [37], are unsuitable since the evaluation of decoding models requires the comparison between two images that could be dissimilar to each other.

To validate the above question, we collected human ratings on the semantic similarities of 1,000 ground-truth (GT) and reconstruction pairs from 22 evaluators. Using these ratings, we reveal that most existing metrics show a low correlation with human judgments about the semantic similarity of GT and its brain-decoded reconstruction, with the exception of EffNet [34]. Our finding underscores the urgent need for improved evaluation criteria.

To that end, we propose a new evaluation metric that primarily focuses on the semantic likeness of two images, SEED (**S**emantic **E**valuation for **V**isual **B**rain **D**ecoding). SEED integrates two newly proposed metrics, *Object F1* and *Cap-Sim*, alongside EffNet, each capturing different aspects of semantic information. More specifically, Object F1 leverages MM-Grounding-DINO [44], a state-of-the-art open-vocabulary image grounding model, to identify and capture the key objects essential to the semantics of each image, enabling an automated assessment of *object presence* in reconstructions. Cap-Sim measures caption similarity by utilizing image captions generated with GIT [35] and computing the semantic similarity using Sentence Transformer [26]. This metric captures additional semantic factors that might be overlooked by Object F1, such as *backgrounds, pose and color*, offering a more comprehensive evaluation of the image semantics. Moreover, these metrics are inherently interpretable to humans and do not rely on a comparison image pool, allowing it to independently assess the quality of reconstructed images. We also integrate EffNet—a currently adopted metric that demonstrates a strong correlation with human assessments—into SEED. Leveraging an ImageNet [5] pre-trained model, EffNet is particularly well-suited to capturing additional aspects such as *style or global scene information*, thus complementing Object F1 and Cap-Sim with broader insights.

Our evaluation results show that each component of SEED exhibits strong agreement with human judgments while focusing on different aspects of an image, and notably, SEED achieves the highest agreement with human ratings compared to existing metrics and other possible alternative methods. In addition, SEED reveals that even the most advanced decoding models often fail to accurately reproduce key objects of interest, frequently mistaking them for similar objects. Furthermore, we will release the human survey results to facilitate future research on developing new evaluation metrics.

Additionally, we introduce a novel loss function, exper-

imentally shown to effectively align brain-predicted CLIP image embeddings with their corresponding GT image embeddings. This alignment leads to improvements not only in the current metrics but also in SEED. Moreover, our loss is compatible with decoding models that use mean squared error as their main objective, making it broadly applicable to existing models such as MindEye [29, 30], MindBridge [36], and UniBrain [38].

In summary, our contributions are three-fold:

- **Comprehensive Semantic Evaluation Metric:** We propose SEED, a novel evaluation metric integrating Object F1, Cap-Sim, and EffNet to assess the semantic similarity between GT and reconstructed images. Object F1 quantifies key object presence, while Cap-Sim and EffNet capture other aspects of semantic information, such as background, pose, color, style, and texture. By integrating these metrics, SEED achieves the best agreement with human judgments.
- **The Release of Human Evaluation Results:** We will open-source the human evaluation results to encourage research on developing more advanced metrics to evaluate the decoding models.
- **Novel Loss Term for Better Embedding Alignment:** To improve the performance of decoding models, we introduce a novel loss that facilitates the alignment between brain-predicted CLIP image embeddings with the GT counterparts. We experimentally show that our proposed loss consistently enhances the semantic decoding performance of current decoding models while it is compatible with models like MindEye [29, 30], MindBridge [36], and UniBrain [38].

2. Background

2.1. Visual brain decoding models

In the early stage of development of visual decoding models, linear regression-based approaches demonstrated that visual information can be decoded from brain signals [9, 12]. With the development of deep learning techniques, more sophisticated decoding becomes promising, such as GAN [8] based visual brain decoding [23, 31].

Recent decoding models adopt latent diffusion models [27, 41] to produce high-quality decoded images conditioned by brain embedding or predicted CLIP [24] embeddings from fMRI signals [2, 4, 29, 30, 36, 38, 39]. MindEye [29, 30] utilize the diffusion prior [25] to predict the CLIP image embedding of visual stimuli and reconstruct the visual stimuli in high quality compared to previous works. MindBridge [36] introduced a subject-unified decoding model by max-pooling fMRI signals from each subject to make inputs of equal size. Then, they adopt a subject-wise encoder to project the information of brain signals to a shared latent space. The projected latent is then

transformed to the shape of CLIP embedding and aligned with CLIP image and text embeddings. To eliminate reliance on subject-specific encoders, UniBrain [38] introduces three distinct extractors that derive geometric, semantic, and mutual global representations from brain signals. The extracted information are subsequently processed by transformer-based embedders to align with CLIP image and text embeddings. Instead of freezing the pre-trained diffusion models, NeuroPictor [11] fine-tunes the diffusion model to directly condition the image generation process with brain embeddings.

2.2. Current evaluation schemes

Most of the recent decoding literature [11, 18, 22, 29, 30, 32, 36, 38, 39] mainly focus on the following eight evaluation metrics: PixCorr, SSIM [37], AlexNet(2), AlexNet(5) [13], Inception [33], CLIP [24], EffNet [34], and SwAV [3].

PixCorr refers to the Pearson correlation between the pixel values of the GT and the reconstruction. SSIM refers to the structural similarity index measure between the GT and the reconstruction.

AlexNet(2), AlexNet(5), Inception, and CLIP refer to the accuracy of two-way identification tasks that use the corresponding feature extractor. Specifically, for every GT embedding, the Pearson correlation with its corresponding reconstruction embedding is compared against its correlation with each other reconstruction embedding in the test set. The percentage of cases in which the GT embedding is closer to its correct reconstruction is reported.

The n-way extension of the task utilizing the brain-generated intermediate CLIP embeddings and the GT CLIP image embeddings, known as image/brain retrieval, is also reported in some works [15, 29, 30]. However, the retrieval tasks are not applicable to models such as NeuroPictor [11] as it requires the model to generate brain-derived intermediate CLIP image embeddings during the decoding process.

EffNet and SwAV refer to the correlation distance between the GT embedding and the reconstruction embedding, utilizing the corresponding feature extractor.

PixCorr, SSIM, AlexNet(2), and AlexNet(5) are considered as “low-level” metrics that focus on lower-level perceptual features. Meanwhile, Inception, CLIP, EffNet, and SwAV are considered as “high-level” metrics that focus on higher-level properties such as semantics.

3. Issues with Existing Evaluation Methods

3.1. Evaluation with metrics from relevant domains

When evaluating visual brain decoding models, it is crucial to measure how closely the reconstruction aligns with the (known) GT, acknowledging potential perceptual and semantic deviations. Unlike typical image generation tasks—which lack a fixed GT—decoding tasks involve a

predetermined target. Consequently, standard metrics for image generation, such as FID, are unsuitable, and a measure that directly compares the reconstruction to the known image is required.

In this sense, due to the nature of comparing the similarity of two images, the evaluation of the decoding task more closely resembles traditional image quality assessment, where images are degraded by compression, transmission, or other processes. This is precisely the context for which metrics like SSIM were originally designed for and likely the reason why those metrics are widely used for the evaluation of visual brain decoding models.

However, a key distinction lies in the inherent noisiness of decoding, which can yield reconstructions that deviate perceptually from the GT while retaining a similar semantic theme. This can result in metrics like SSIM assigning unusually low scores as they are prone even to small distortions such as translations and rotations [20], not to mention ones found in the reconstructions.

Consequently, although it might appear that conventional image quality assessment metrics are ideally suited to evaluate decoding models, in practice, they are substantially misaligned from human judgments, as demonstrated in Sec. 6.2. Therefore, the focus of evaluation should be geared towards assessing the semantic qualities of the reconstructions, due to the noisiness of the decoding process.

3.2. Two-way identification

Two-way identification metrics (AlexNet(2), AlexNet(5), Inception, CLIP) serve a crucial role in the evaluation of decoding models, as they occupy half of the eight-metric evaluation scheme. However, due to their comparative nature, two-way identification metrics contain some inherent flaws. First and foremost, comparing two-way identification scores between models is inappropriate. As each reconstruction is compared against other reconstructions generated by the decoding model, the pool of images each reconstruction is compared against differs for each decoding model. This fact renders the direct comparison of two-way identification scores inappropriate, as each model would be evaluated under different criteria.

Another issue arises from the difficulty, or lack thereof, of the two-way identification task. Since the reconstruction only needs to be closer to the GT than another random example, a reasonable reconstruction easily “wins” the comparison. Due to this, recent decoding models already show near-perfect performance for most two-way identification metrics. This makes it difficult to differentiate the performance between different decoding models and thus calls for a more challenging evaluation task.

3.3. Lack of human-likeness

Excluding PixCorr and SSIM, all other evaluation metrics rely on abstract features extracted from pre-trained vision models. Consequently, it is difficult to interpret the rationale behind each evaluation from a human perspective, casting doubt on whether they truly align with human perception—especially while under scrutiny. Indeed, our human survey findings reveal that most commonly used metrics gauge semantic similarity in ways that deviate notably from human judgments. Further details are provided in Sec. 6.2.

4. Semantic Evaluation for Visual Brain Decoding

Given the problems outlined in Sec. 3, there is a clear need for evaluation methods that deliver more accurate and generalizable assessments. To this end, we propose the following evaluation methods: Object F1, Cap-Sim, and SEED.

4.1. Object F1

One basic criterion for a semantically correct reconstruction should be the existence of key objects; that is, objects present in the GT should also be present in the reconstruction, and objects not present in the GT should also not be present in the reconstruction. Using image grounding models, it is possible to automatically detect the objects present in the GT and the reconstruction and quantify the aforementioned criterion into two proposed metrics: Object Recall and Object Precision.

We first run all GT and reconstructed images through an image grounding model and obtain the detection results. The results should contain the list of detected objects with information such as the category and the confidence value for each object. Given a confidence threshold t , which is the threshold used to determine whether an object is “detected,” we define two preliminary metrics for each image: Object Recall $_t$ and Object Precision $_t$.

Object Recall $_t$ measures the proportion of the object categories from the GT that are also present in the reconstruction. This measures the proportion of objects that are successfully “recalled” in the reconstruction, formulated as:

$$\text{Object Recall}_t := \frac{\# \text{ of categories in both GT and recon}}{\# \text{ of categories in GT}} \quad (1)$$

Similarly, Object Precision $_t$ measures the proportion of the object categories from the reconstruction that are also present in the GT. This essentially measures the “precision” of the objects in the reconstruction, formulated as:

$$\text{Object Precision}_t := \frac{\# \text{ of categories in both GT and recon}}{\# \text{ of categories in recon}} \quad (2)$$

During the process, we apply the same threshold value to the GT and reconstruction to ensure the ideal reconstruction (i.e., reconstruction identical to the GT) obtains the best possible score. For simplicity, if multiple objects of the same category are present in an image, additional objects are not considered while calculating the metrics, as we only check for the existence of each object category.

To remove the reliance on a threshold hyperparameter, we calculate Object Recall $_t$ and Object Precision $_t$ while moving the threshold value, t , between 0 and 1 and obtain the averaged values:

$$\begin{aligned} \text{Object Recall} &:= \frac{1}{t_{\text{valid}}^{\text{recall}}} \int_0^{t_{\text{valid}}^{\text{recall}}} \text{Object Recall}_t dt \\ \text{Object Precision} &:= \frac{1}{t_{\text{valid}}^{\text{precision}}} \int_0^{t_{\text{valid}}^{\text{precision}}} \text{Object Precision}_t dt \end{aligned} \quad (3)$$

where $t_{\text{valid}}^{\text{recall}}, t_{\text{valid}}^{\text{precision}}$ are cutoff thresholds, corresponding to the highest confidence value present in the GT and reconstruction, respectively. The threshold is cut off in such a way since there would be no detected objects for higher threshold values.

The final evaluation metric, Object F1, is the harmonic mean of the averaged Object Recall and Object Precision:

$$\text{Object F1} := \frac{2}{\text{Object Recall}^{-1} + \text{Object Precision}^{-1}} \quad (4)$$

The threshold-averaging scheme has the added benefit of penalizing reconstructions with objects far apart from the GT regarding the confidence score, as those objects would be marked as incorrect during the intermediate threshold values. This trait is beneficial for evaluating decoding models, as they often generate distorted objects [30] that tend to show lower confidence values than their GT counterparts.

To calculate Object F1, we employ MM-Grounding-DINO [44] to detect the objects and provide 82 possible object categories; the full list of categories is available in Sec. B. For Object Recall and Object Precision, to approximate Eq. (3), we move the threshold t from 0 by increments of 0.01, up to the cutoff thresholds and average the values, and the resulting Object F1 is calculated for each image.

4.2. Cap-Sim

Another approach to assessing the semantic similarity of two images is to measure the similarity between captions generated by image captioning models for each GT and reconstruction pair. Instead of relying on abstract features generated by vision models, this approach emphasizes semantic qualities expressible by natural language since the images are essentially “compressed” into text before being compared. This method allows us to evaluate semantic factors that are hard to identify through the existence of objects, such as the background information or attributes of

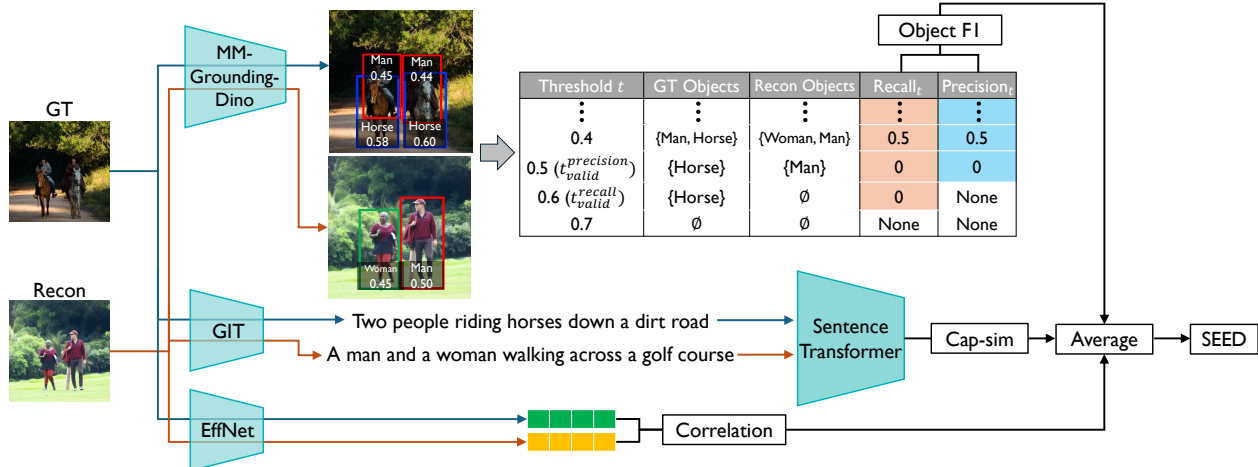


Figure 2. The overall process for calculating SEED.

the detected object (pose, color, etc.). Furthermore, caption-based evaluation provides an interpretable assessment of model performance, as captions are human-readable and closely align with how people describe visual content [10].

Formally, Cap-Sim is formulated as:

$$\text{Cap-Sim} := \cos(e_{\text{text}}(c(I_{GT})), e_{\text{text}}(c(I_{recon}))) \quad (5)$$

where I_{GT} and I_{recon} are GT and reconstructions, respectively. The function $e_{\text{text}}(\cdot)$ is a text encoder; in our case, we use Sentence Transformer [26]. $c(\cdot)$ is a caption generator; in our case, we use GIT [35].

4.3. SEED

We hypothesize that combining several distinct high-performing metrics, in terms of alignment with human judgments, can yield superior metrics by supplementing each other’s misjudgments. Doing so will result in a comprehensive and unified measure that can serve as the go-to metric for evaluating decoding models. To that end, we present **Semantic Evaluation of Visual Brain Decoding (SEED)**, a metric that combines Object F1, Cap-Sim, and $\overline{\text{EffNet}}$. We integrate $\overline{\text{EffNet}}$ alongside the proposed metrics as it shows strong agreement with human judgments (can be checked from Tab. 1) and has a possibility of capturing additional aspects of images coming from the ImageNet [5] pre-trained model. The overall procedure to compute SEED for a GT and reconstruction pair is depicted in Fig. 2. We simply take the average of the three metrics to calculate SEED,

$$\text{SEED} := (\text{Object F1} + \text{Cap-Sim} + \overline{\text{EffNet}}) / 3 \quad (6)$$

Note that $\overline{\text{EffNet}}$ is a slightly modified metric by calculating **correlation**, not **correlation distance**, converting it into a higher-is-better metric like the other two;

$$\overline{\text{EffNet}} := \text{corr}(e_{\text{img}}(I_{GT}), e_{\text{img}}(I_{recon})) \quad (7)$$

where the function $e_{\text{img}}(\cdot)$ is the image encoder, EffNet.

In Sec. 6.3, we empirically show the rationale behind the choice of three metrics (Object F1, Cap-Sim, $\overline{\text{EffNet}}$), as the combination between those three high-performing metrics showed noticeable improvements compared to the individual metrics themselves.

4.4. Human evaluation of image similarity

We collected 5-Likert scale ratings from 22 human evaluators to assess the alignment of current evaluation metrics with human judgments. They assessed both the semantic and perceptual similarity between GT and their reconstructions for 1,000 test set images used in [30], where the reconstructions were generated by the MindEye2 model released by the original author, with 250 reconstructions sequentially sampled from each of the four subjects (subject 1,2,5, and 7), following the order: the first 250 from subject 1, the next 250 from subject 2, and so on. The detailed information on the collection of human ratings is provided in Sec. A, and we will release the survey results to facilitate future research on developing new sophisticated evaluation frameworks.

5. Pairwise Hinge Loss

To enhance the semantic decoding capabilities of existing decoding models, we introduce a novel loss term: a straightforward approach which involves reducing the distance between the CLIP image embeddings of the GT images and those predicted from brain signals. Note that some previous works implement a distillation-based loss, known as *SoftCLIP*, to effectively bridge the gap between GT CLIP embeddings and brain-predicted embeddings [29, 30, 36]; further details can be found in [36].

For a more accurate alignment, we hypothesize that incorporating the order information of cosine similarities among different samples into the training process can provide rich insights into the geometry of CLIP’s embedding space. To be precise, let $t_i \in \mathbb{R}^d, 1 \leq i \leq N$ be the d -dimensional GT CLIP image embeddings where N is the

batch size. Then, let $p_i \in \mathbb{R}^d$, $1 \leq i \leq N$ be corresponding predicted embeddings from brain signals. The rationale of our proposed loss term is to impose a penalty if the order relationship is violated in p_i compared to t_i . That is, whenever $\cos(p_i, t_j) > \cos(p_i, t_k)$ and $\cos(t_i, t_j) < \cos(t_i, t_k)$, we consider a loss amount of $\cos(p_i, t_j) - \cos(p_i, t_k)$ where $1 \leq i, j, k \leq N$. We dub this loss as pairwise hinge loss, mathematically formulated as

$$\mathcal{L}_{\text{pair}} := \frac{1}{N^2(N-1)} \sum_{i,j,k} \{ \max(0, \cos(p_i, t_j) - \cos(p_i, t_k)) \cdot \mathbf{1}(\cos(t_i, t_j) < \cos(t_i, t_k)) \} \quad (8)$$

where $\mathbf{1}(\cdot)$ is the indicator function.

We use the $\mathcal{L}_{\text{pair}}$ alongside the original training objective of each decoding model, which makes the training objective $\mathcal{L}_{\text{baseline}} + \lambda_{\text{pair}} \mathcal{L}_{\text{pair}}$, where the $\mathcal{L}_{\text{baseline}}$ is exactly adopted from the baseline, and the λ_{pair} is a weighting hyperparameter. Empirically, we found that applying the $\mathcal{L}_{\text{pair}}$ for a certain period of training is effective, so we adopt additional hyperparameter T_{pair} to adjust the number of epochs where the $\mathcal{L}_{\text{pair}}$ is applied from the beginning.

6. Experimental Results

6.1. Dataset description

We use the Natural Scenes Dataset (NSD) [1] in our experiments, following prior works [29, 30, 36, 38]. The dataset consists of 7T fMRI recordings collected while subjects viewed natural images from the MS-COCO dataset [16].

NeuroPictor [11], MindBridge [36], and UniBrain [38] utilize data from only four subjects (subj 1, 2, 5, and 7) who completed all sessions, as done in MindEye1 [29]. This subset includes 982 unique images for the test set, 8,559 distinct images for the training set, and 300 for the validation set. In contrast, MindEye2 [30] incorporates data from all eight subjects, using seven for pre-training and the remaining one for fine-tuning. Due to the sequential disclosure of the NSD dataset, there are discrepancies in the number of images used across prior works. The original implementation of MindEye2 uses 9,000 distinct images for training and 1,000 for testing.

To ensure consistency with [11, 36, 38] for hyperparameter selection in Sec. 6.6, we split the dataset accordingly, resulting in 8,700 training images and 300 validation images. After the hyperparameter search, we merged the train and validation splits to train the final model for all methods discussed in Sec. 6.6.

6.2. Alignment with human judgments

Following [17], we adopt pairwise accuracy [6], Kendall’s Tau-b, and Pearson correlation to meta-evaluate each metric based on the human ratings on the semantic similarity

Metric	Pairwise Acc.	Kendall	Pearson
PixCorr	53.8%	.075	.117
SSIM [37]	54.5%	.090	.112
AlexNet(2) [13]	55.0%	.185	.187
AlexNet(5) [13]	49.5%	.236	.258
Inception [33]	63.8%	.330	.475
CLIP [24]	66.4%	.368	.436
EffNet [34]	78.0%	.559	.748
SwAV [3]	69.7%	.394	.576
BLIP Cap-Sim [14, 26]	73.5%	.471	.670
BLIP FlanT5 [14, 17]	71.3%	.427	.566
GIT FlanT5 [17, 35]	71.5%	.430	.571
Object F1	75.8%	.516	.708
Cap-Sim	73.8%	.477	.683
SEED	81.0%	.621	.817

Table 1. The meta-evaluation results of each metric. The best results are **bolded**. Note that SwAV was calculated similarly to Eq. (7) to also convert it into a higher-is-better metric.

between images. We meta-evaluated eight metrics widely used in prior works [29, 30, 36, 38]. Additionally, we explored alternative approaches for measuring the semantic similarity between images: BLIP [14] caption similarity using Sentence Transformer [26] and CLIP-FlanT5 VQA scores [17] with BLIP/GIT generated captions for GT images.

The meta-evaluation results, presented in Tab. 1, indicate that most existing evaluation metrics exhibit low correlation with human judgments, except for EffNet. Furthermore, the alternative approaches do not perform as effectively as Object F1 or Cap-Sim. Notably, SEED achieves the highest agreement with human judgments.

6.3. Combination of evaluation metrics

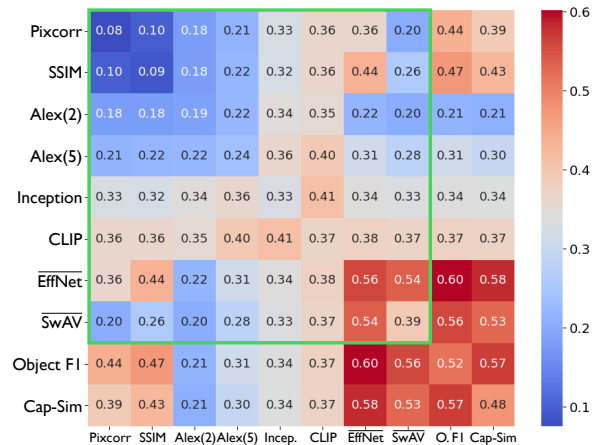


Figure 3. The heatmap of correlations between metric combinations and human evaluation, measured by Kendall’s Tau-b. The green outline indicates combinations within current metrics.

To investigate possible candidate metrics that could be included in SEED, we computed the correlation with human evaluations for each possible metric combination, as shown in Fig. 3. The combination is calculated by simply averaging the two metrics. The highest-performing metrics come from the combination of Object F1, Cap-Sim, and $\overline{\text{EffNet}}$, with each combination outperforming the individual components. This result naturally prompts the combination of those three to obtain SEED.

One interesting observation is that it is impossible to create a superior evaluation metric by combining existing metrics; all possible combinations within existing metrics are not better than standalone $\overline{\text{EffNet}}$. A better metric emerges only when combined with Object F1 or Cap-Sim. We believe that this is one indirect evidence that our proposed metrics evaluate the reconstructions from a different angle from EffNet, making it possible for them to work as a complementary metric for each other.

6.4. Analysis of worst-case judgments


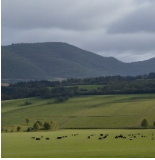




(a)			Metric	Rank
			Human	230
			Object F1	995
			Cap-Sim	484
			EffNet	113
(b)			Metric	Rank
			Human	2
			Object F1	216
			Cap-Sim	629
			EffNet	21
(c)			Metric	Rank
			Human	270
			Object F1	352
			Cap-Sim	421
			EffNet	964

Figure 4. Examples and rankings (out of 1000 pairs) of worst-case judgments for (a) Object F1, (b) Cap-Sim, and (c) EffNet.

Metric	Average Score	
	Same Class	Diff. Class
$\overline{\text{EffNet}}$	0.755	-0.333
Human	0.313	-0.138

Table 2. Average normalized score of EffNet and Human evaluations for images with the same/different ImageNet predictions.

To understand why SEED improves upon its components, we present case studies of the “worst-case judgments” for each component of SEED, despite their high agreement with human judgments. In this context, “worst-case judgments” refer to images whose metric-based ranking differs significantly from the human evaluation ranking. The examples shown in Fig. 4 are chosen among the



Figure 5. Examples of the semantic near-miss phenomenon

worst-case judgments for each metric, where the other two metrics made a reasonably human-aligned decision which somewhat mitigates the discrepancy. Additional examples are available in Sec. E.

Fig. 4 (a) illustrates a case where Object F1 significantly deviates from human evaluation by assigning a score of 0. This disparity arises because Object F1 fails to capture the global scene information, relying solely on detected animals (*sheep* in the GT and *cow* in the reconstruction).

Fig. 4 (b) depicts a case where Cap-Sim produces a low similarity between the two images, where the caption generated by GIT is [A man skiing down a snowy slope with a lot of trees in the background.] and [A woman is skiing down a snowy hill.] for the GT and the reconstruction, respectively. The low similarity likely results from the change of the person’s gender, alongside additional details [with a lot of trees in the background.] for the GT caption.

Fig. 4 (c) shows a case where $\overline{\text{EffNet}}$ produces a drastically low correlation between the two images. One possible reason is that the two images have different ImageNet Top-1 predictions from the EffNet model: *American egret* for the GT and *Coucal* for the reconstruction. We hypothesize that the EffNet tends to overestimate the correlation between two images with the same class prediction and, conversely, underestimate the correlation between two images with different class predictions.

To validate this assumption, at Tab. 2, we compare the average $\overline{\text{EffNet}}$ and the human semantic evaluation scores of the image pairs with the same/different EffNet ImageNet Top-1 predictions. Note that EffNet and human scores are z-normalized for a fair comparison. We indeed found that $\overline{\text{EffNet}}$ tends to assess the similarity between two images in a more extreme manner than humans do. We believe this explains EffNet’s low correlation in the case of Fig. 4 (c).

Method	$\mathcal{L}_{\text{pair}}$	Low-level				High-Level				Object F1 \uparrow	Cap-Sim \uparrow	SEED \uparrow
		PixCorr \uparrow	SSIM \uparrow	Alex(2) \uparrow	Alex(5) \uparrow	Incep \uparrow	CLIP \uparrow	EffNet \downarrow	SwAV \downarrow			
MindEye2 [30]	\times	.268	.381	95.4%	98.5%	94.5%	93.0%	.626	.348	.507	.541	.474
	\checkmark	.267	.382	95.2%	98.5%	94.6%	93.3%	.625	.347	.509	.541	.475
MindBridge [36]	\times	.161	.278	88.3%	95.5%	91.8%	94.1%	.696	.410	.440	.486	.410
	\checkmark	.160	.272	88.3%	95.6%	92.1%	94.2%	.684	.405	.460	.496	.424
UniBrain [38]	\times	.138	.260	84.4%	93.7%	88.8%	91.5%	.721	.426	.403	.462	.381
	\checkmark	.146	.253	85.4%	94.1%	89.5%	92.0%	.718	.422	.410	.469	.387

Table 3. Quantitative results with reproduced models and with $\mathcal{L}_{\text{pair}}$.

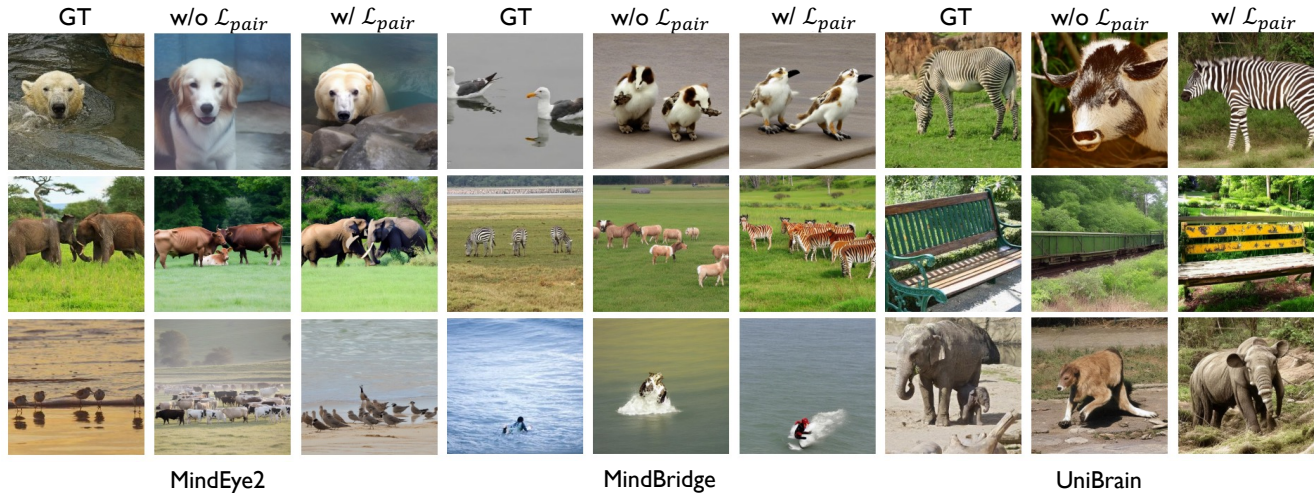


Figure 6. Qualitative results of subject 1 with reproduced models and with $\mathcal{L}_{\text{pair}}$.

6.5. Semantic near-miss phenomenon

One common failure mode of current decoding models is the *semantic near-miss* phenomenon, in which the reconstruction misrepresents the specific object category from the GT, yet still captures the broader supercategory. For example, if the GT contains a *dog*, the reconstruction might include a *cat* or other animals (See Fig. 5.). While this *cat* is wrong at the object category level, it remains within the correct supercategory, *animal*.

We quantify the phenomenon by re-using the object detection pipeline used in Object F1. We calculate the Object Recall (Eq. (1)) and the *Relaxed* Object Recall, which measures the proportion of the object categories from the GT where its supercategory (instead of the specific category) is present in the reconstruction. The gap between those two represents the rate of the semantic near-miss phenomenon.

We computed the semantic near-miss rate of salient object categories [40] at a confidence threshold of 0.3 for four existing decoding models—MindEye2, NeuroPictor, MindBridge, and UniBrain—and observed rates of 0.175, 0.191, 0.203, and 0.206, respectively. Such a high incidence indicates that current decoding models often struggle with fine-grained object differentiation, capturing only coarse semantic details. Addressing this issue could be a promising avenue for future research, potentially yielding more precise

and semantically faithful reconstructions.

6.6. Effects of the pairwise hinge loss

To demonstrate the effectiveness of the $\mathcal{L}_{\text{pair}}$ in enhancing brain decoding performance and its applicability to various methods, we reproduced the baseline methods ourselves and applied the $\mathcal{L}_{\text{pair}}$ during their training. The experimental details are summarized in Sec. C.1.

Tab. 3 presents our quantitative findings, while the qualitative outcomes appear in Fig. 6 (with additional examples provided in Sec. C.2). For the qualitative results, we highlight cases where SEED benefits the most from the $\mathcal{L}_{\text{pair}}$. As demonstrated, the $\mathcal{L}_{\text{pair}}$ significantly enhances semantic decoding both numerically and visually.

7. Conclusion & Limitations

In this work, we introduce **SEED**, a novel evaluation metric and framework designed to assess the semantic decoding performance of decoding models. Through comprehensive experiments, we reveal that existing evaluation metrics often diverge from human judgment, while our proposed metric demonstrates more consistent alignment and improved accuracy. Additionally, we open-source the human evaluation results to encourage future research on developing more advanced evaluation frameworks for decoding mod-

els. Furthermore, we propose **pairwise hinge loss**, a novel loss term that enhances alignment between the image embeddings of the GT and its reconstruction, consistently improving the performance of existing decoding models.

However, our approach has some limitations in that SEED does not account for perceptual aspects. We hope that future research will build upon our open-source human survey results to develop more refined evaluation metrics.

References

- [1] Emily J Allen, Ghislain St-Yves, Yihan Wu, Jesse L Breedlove, Jacob S Prince, Logan T Dowdle, Matthias Nau, Brad Caron, Franco Pestilli, Ian Charest, et al. A massive 7t fmri dataset to bridge cognitive neuroscience and artificial intelligence. *Nature neuroscience*, 25(1):116–126, 2022. 6
- [2] Johann Banchetrit, Hubert Banville, and Jean-Rémi King. Brain decoding: toward real-time reconstruction of visual perception. *arXiv preprint arXiv:2310.19812*, 2023. 2
- [3] Mathilde Caron, Ishan Misra, Julien Mairal, Priya Goyal, Piotr Bojanowski, and Armand Joulin. Unsupervised learning of visual features by contrasting cluster assignments. *Advances in neural information processing systems*, 33:9912–9924, 2020. 3, 6
- [4] Zijiao Chen, Jiaxin Qing, Tiange Xiang, Wan Lin Yue, and Juan Helen Zhou. Seeing beyond the brain: Conditional diffusion model with sparse masked modeling for vision decoding. In *Proceedings of the IEEE/CVF Conference on Computer Vision and Pattern Recognition*, pages 22710–22720, 2023. 1, 2
- [5] Jia Deng, Wei Dong, Richard Socher, Li-Jia Li, Kai Li, and Li Fei-Fei. Imagenet: A large-scale hierarchical image database. In *2009 IEEE conference on computer vision and pattern recognition*, pages 248–255. Ieee, 2009. 2, 5
- [6] Daniel Deutsch, George Foster, and Markus Freitag. Ties matter: Meta-evaluating modern metrics with pairwise accuracy and tie calibration. *arXiv preprint arXiv:2305.14324*, 2023. 6
- [7] Bing Du, Xiaomu Cheng, Yiping Duan, and Huansheng Ning. fmri brain decoding and its applications in brain-computer interface: A survey. *Brain Sciences*, 12(2):228, 2022. 1
- [8] Ian Goodfellow, Jean Pouget-Abadie, Mehdi Mirza, Bing Xu, David Warde-Farley, Sherjil Ozair, Aaron Courville, and Yoshua Bengio. Generative adversarial networks. *Communications of the ACM*, 63(11):139–144, 2020. 2
- [9] John-Dylan Haynes and Geraint Rees. Predicting the orientation of invisible stimuli from activity in human primary visual cortex. *Nature neuroscience*, 8(5):686–691, 2005. 2
- [10] Sen He, Hamed R Tavakoli, Ali Borji, and Nicolas Pugeault. Human attention in image captioning: Dataset and analysis. In *Proceedings of the IEEE/CVF International Conference on Computer Vision*, 2019. 5
- [11] Jingyang Huo, Yikai Wang, Yun Wang, Xuelin Qian, Chong Li, Yanwei Fu, and Jianfeng Feng. Neuropictor: Refining fmri-to-image reconstruction via multi-individual pretraining and multi-level modulation. In *European Conference on Computer Vision*, pages 56–73. Springer, 2024. 1, 3, 6, 14
- [12] Yukiyasu Kamitani and Frank Tong. Decoding the visual and subjective contents of the human brain. *Nature neuroscience*, 8(5):679–685, 2005. 2
- [13] Alex Krizhevsky, Ilya Sutskever, and Geoffrey E Hinton. Imagenet classification with deep convolutional neural networks. *Advances in neural information processing systems*, 25, 2012. 3, 6
- [14] Junnan Li, Dongxu Li, Silvio Savarese, and Steven Hoi. Blip-2: Bootstrapping language-image pre-training with frozen image encoders and large language models. In *International conference on machine learning*, pages 19730–19742. PMLR, 2023. 6
- [15] Sikun Lin, Thomas Sprague, and Ambuj K. Singh. Mind Reader: Reconstructing complex images from brain activities, 2022. 1, 3
- [16] Tsung-Yi Lin, Michael Maire, Serge Belongie, James Hays, Pietro Perona, Deva Ramanan, Piotr Dollár, and C Lawrence Zitnick. Microsoft coco: Common objects in context. In *Computer Vision—ECCV 2014: 13th European Conference, Zurich, Switzerland, September 6–12, 2014, Proceedings, Part V 13*, pages 740–755. Springer, 2014. 6
- [17] Zhiqiu Lin, Deepak Pathak, Baiqi Li, Jiayao Li, Xide Xia, Graham Neubig, Pengchuan Zhang, and Deva Ramanan. Evaluating text-to-visual generation with image-to-text generation, 2024. 6
- [18] Yulong Liu, Yongqiang Ma, Guibo Zhu, Haodong Jing, and Nanning Zheng. See Through Their Minds: Learning Transferable Neural Representation from Cross-Subject fMRI, 2024. 3
- [19] Weijian Mai, Jian Zhang, Pengfei Fang, and Zhijun Zhang. Brain-conditional multimodal synthesis: A survey and taxonomy. *IEEE Transactions on Artificial Intelligence*, 2024. 1
- [20] Jim Nilsson and Tomas Akenine-Möller. Understanding SSIM, 2020. 3
- [21] Mayu Otani, Riku Togashi, Yu Sawai, Ryosuke Ishigami, Yuta Nakashima, Esa Rahtu, Janne Heikkilä, and Shin’ichi Satoh. Toward verifiable and reproducible human evaluation for text-to-image generation. In *Proceedings of the IEEE/CVF Conference on Computer Vision and Pattern Recognition*, pages 14277–14286, 2023. 11
- [22] Furkan Ozelik and Rufin VanRullen. Natural scene reconstruction from fMRI signals using generative latent diffusion, 2023. 3
- [23] Furkan Ozelik, Bhavin Choksi, Milad Mozafari, Leila Reddy, and Rufin VanRullen. Reconstruction of perceived images from fmri patterns and semantic brain exploration using instance-conditioned gans. In *2022 International Joint Conference on Neural Networks (IJCNN)*, pages 1–8. IEEE, 2022. 2
- [24] Alec Radford, Jong Wook Kim, Chris Hallacy, Aditya Ramesh, Gabriel Goh, Sandhini Agarwal, Girish Sastry, Amanda Askell, Pamela Mishkin, Jack Clark, et al. Learning transferable visual models from natural language supervision. In *International conference on machine learning*, pages 8748–8763. PMLR, 2021. 2, 3, 6

- [25] Aditya Ramesh, Prafulla Dhariwal, Alex Nichol, Casey Chu, and Mark Chen. Hierarchical text-conditional image generation with clip latents. *arXiv preprint arXiv:2204.06125*, 1(2):3, 2022. 2
- [26] Nils Reimers and Iryna Gurevych. Sentence-bert: Sentence embeddings using siamese bert-networks. In *Proceedings of the 2019 Conference on Empirical Methods in Natural Language Processing*. Association for Computational Linguistics, 2019. 2, 5, 6
- [27] Robin Rombach, Andreas Blattmann, Dominik Lorenz, Patrick Esser, and Björn Ommer. High-resolution image synthesis with latent diffusion models. In *Proceedings of the IEEE/CVF conference on computer vision and pattern recognition*, pages 10684–10695, 2022. 2
- [28] Simanto Saha, Khondaker A Mamun, Khawza Ahmed, Raqibul Mostafa, Ganesh R Naik, Sam Darvishi, Ahsan H Khandoker, and Mathias Baumert. Progress in brain computer interface: Challenges and opportunities. *Frontiers in systems neuroscience*, 15:578875, 2021. 1
- [29] Paul S. Scotti, Atmadeep Banerjee, Jimmie Goode, Stepan Shabalin, Alex Nguyen, Ethan Cohen, Aidan J. Dempster, Nathalie Verlinde, Elad Yundler, David Weisberg, Kenneth A. Norman, and Tanishq Mathew Abraham. Reconstructing the Mind’s Eye: fMRI-to-Image with Contrastive Learning and Diffusion Priors, 2023. 1, 2, 3, 5, 6
- [30] Paul S. Scotti, Mihir Tripathy, Cesar Kadir Torrico Vilanueva, Reese Kneeland, Tong Chen, Ashutosh Narang, Charan Santhirasegaran, Jonathan Xu, Thomas Naselaris, Kenneth A. Norman, and Tanishq Mathew Abraham. Mind-Eye2: Shared-Subject Models Enable fMRI-To-Image With 1 Hour of Data, 2024. 1, 2, 3, 4, 5, 6, 8, 11, 14
- [31] Katja Seeliger, Umut Güçlü, Luca Ambrogioni, Yagmur Güçlütürk, and Marcel AJ Van Gerven. Generative adversarial networks for reconstructing natural images from brain activity. *NeuroImage*, 181:775–785, 2018. 2
- [32] Guobin Shen, Dongcheng Zhao, Xiang He, Linghao Feng, Yiting Dong, Jihang Wang, Qian Zhang, and Yi Zeng. Neuro-Vision to Language: Image Reconstruction and Language enabled Interaction via Brain Recordings, 2024. 3
- [33] Christian Szegedy, Wei Liu, Yangqing Jia, Pierre Sermanet, Scott Reed, Dragomir Anguelov, Dumitru Erhan, Vincent Vanhoucke, and Andrew Rabinovich. Going deeper with convolutions. In *Proceedings of the IEEE conference on computer vision and pattern recognition*, pages 1–9, 2015. 3, 6
- [34] Mingxing Tan and Quoc Le. Efficientnet: Rethinking model scaling for convolutional neural networks. In *International conference on machine learning*, pages 6105–6114. PMLR, 2019. 2, 3, 6
- [35] Jianfeng Wang, Zhengyuan Yang, Xiaowei Hu, Linjie Li, Kevin Lin, Zhe Gan, Zicheng Liu, Ce Liu, and Lijuan Wang. Git: A generative image-to-text transformer for vision and language. *arXiv preprint arXiv:2205.14100*, 2022. 2, 5, 6
- [36] Shizun Wang, Songhua Liu, Zhenxiang Tan, and Xinchao Wang. Mindbridge: A cross-subject brain decoding framework. In *Proceedings of the IEEE/CVF Conference on Computer Vision and Pattern Recognition*, pages 11333–11342, 2024. 1, 2, 3, 5, 6, 8, 14
- [37] Zhou Wang, A.C. Bovik, H.R. Sheikh, and E.P. Simoncelli. Image quality assessment: from error visibility to structural similarity. *IEEE Transactions on Image Processing*, 13(4): 600–612, 2004. 2, 3, 6
- [38] Zicheng Wang, Zhen Zhao, Luping Zhou, and Parashkev Nachev. Unibrain: A unified model for cross-subject brain decoding. *arXiv preprint arXiv:2412.19487*, 2024. 1, 2, 3, 6, 8, 11, 14
- [39] Weihao Xia, Raoul de Charette, Cengiz Öztireli, and Jing-Hao Xue. Dream: Visual decoding from reversing human visual system. In *Proceedings of the IEEE/CVF Winter Conference on Applications of Computer Vision*, pages 8226–8235, 2024. 1, 2, 3
- [40] Weihao Xia, Raoul de Charette, Cengiz Öztireli, and Jing-Hao Xue. UMBRAE: Unified Multimodal Brain Decoding, 2024. 8, 11
- [41] Xingqian Xu, Zhangyang Wang, Gong Zhang, Kai Wang, and Humphrey Shi. Versatile diffusion: Text, images and variations all in one diffusion model. In *Proceedings of the IEEE/CVF International Conference on Computer Vision*, pages 7754–7765, 2023. 2
- [42] Bohan Zeng, Shanglin Li, Xuhui Liu, Sicheng Gao, Xiaolong Jiang, Xu Tang, Yao Hu, Jianzhuang Liu, and Baochang Zhang. Controllable mind visual diffusion model. In *Proceedings of the AAAI Conference on Artificial Intelligence*, pages 6935–6943, 2024. 1
- [43] Yingying Zhang, Zhenhao Huang, Yiqing Dai, Yiwen Chen, and Dewen Hu. fmri brain decoding and its applications in brain-computer interface. *Frontiers in Neuroscience*, 16: 869056, 2022. 1
- [44] Xiangyu Zhao, Yicheng Chen, Shilin Xu, Xiangtai Li, Xinjiang Wang, Yining Li, and Haiyan Huang. An Open and Comprehensive Pipeline for Unified Object Grounding and Detection, 2024. 2, 4

SEED: Towards More Accurate Semantic Evaluation for Visual Brain Decoding

Supplementary Material

A. Collection of Human Ratings

We used the Amazon Mechanical Turk (MTurk) platform as well as additional student evaluators to collect human ratings on the semantic and perceptual similarity between GT and its reconstruction. A screenshot of the survey window is shown in Fig. 7.

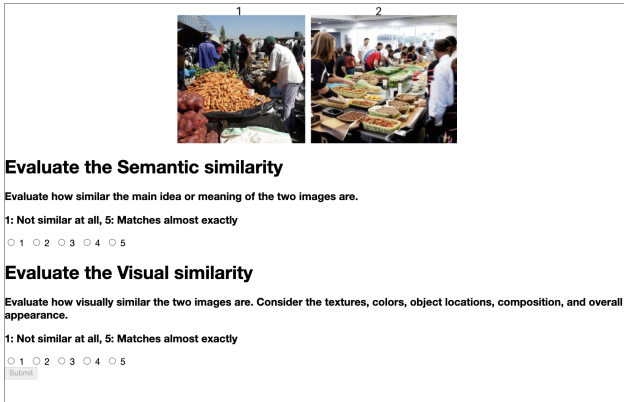


Figure 7. A screenshot of our Amazon MTurk survey window.

Referring to [21], we applied the following filter for worker requirements when creating the MTurk project: 1) Master: Good-performing and granted AMT Masters. Each annotator was paid \$0.03 for evaluating the semantic and perceptual similarity of a single pair of GT and its reconstruction image. We gathered a total of 22 ratings for each of the 1,000 pairs.

B. Full List of Object Categories

The list of object categories, which was used for object detection, is composed of 80 COCO categories plus 2 additional human categories (*man* and *woman*). The resulting 82 categories can be further classified into 30 “Salient” and 52 “Inconspicuous” objects as per [40].

The 30 salient objects are: [person, man, woman, bird, cat, dog, horse, sheep, cow, elephant, bear, zebra, giraffe, bicycle, car, motorcycle, airplane, bus, train, truck, boat, bench, chair, couch, bed, dining table, toilet, sink, refrigerator, clock]

The 52 inconspicuous objects are: [traffic light, fire hydrant, stop sign, parking meter, backpack, umbrella, handbag, tie, suitcase, frisbee, skis, snowboard, sports ball, kite, baseball bat, baseball glove, skateboard, surfboard, tennis racket, bottle, wine glass, cup, fork, knife, spoon, bowl, banana, apple, sandwich, orange, broccoli, carrot, hot dog,

pizza, donut, cake, potted plant, tv, laptop, mouse, remote, keyboard, cell phone, microwave, oven, toaster, book, vase, scissors, teddy bear, hair drier, toothbrush].

C. Experimental Details, Results, and Implementation of Sec. 6.6

C.1. Experimental details

We adopted the same hyperparameters used in each baseline to reproduce, but we reduced the dimension of the shared latent space to 1024 and removed the low-level pipeline in [30] due to the limit of computational resources, following a piece of advice from author. We searched the hyperparameters for $\mathcal{L}_{\text{pair}}$, λ_{pair} and T_{pair} , based on the validation cosine similarity between p_i and t_i . All experiments are conducted with four NVIDIA A100-40GB GPUs.

MindEye2 The original implementation of MindEye2[30] uses 4096-dim of shared latent space and low-level pipeline¹. We searched λ_{pair} from $\{0.33, 0.5, 0.75, 1\}$ and T_{pair} from $\{0.25, 0.5, 0.75\}$.

MindBridge We followed the original implementation². We searched λ_{pair} from $\{0.33, 0.4, 0.5, 0.75\}$ and T_{pair} from $\{0.5, 1.0, 2.0\}$.

UniBrain We followed the original implementation³. We applied the $\mathcal{L}_{\text{pair}}$ only to the alignment between fine geometric embeddings, denoted as e^g in [38], and CLIP image embedding of GT images. We searched λ_{pair} from $\{0.33, 0.5, 0.75\}$ and T_{pair} from $\{5, 10, 15\}$.

C.2. Qualitative results

We present the additional qualitative results of Sec. 6.6 in Fig. 8, Fig. 9, and Fig. 10.

C.3. Python implementation of pairwise hinge loss

```
def pairwise_hinge_loss(preds, targs, temp=5e-3,
                        eps=1e-10):
    # preds : [N, d], targs : [N, d]
    N = preds.shape[0]
    t_t = (targs @ targs.T) / temp + eps
    p_t = (preds @ targs.T) / temp + eps

    # Get pairwise difference matrix
    t_order = torch.sign(t_t[:, :, None] - t_t[:,
        None, :]) # [N, N, N]
    p_t_diff = p_t[:, :, None] - p_t[:, None, :] #
        [N, N, N]

    # Apply penalty only where true_order != 0
```

¹<https://github.com/MedARC-AI/MindEyeV2>

²<https://github.com/littlepure2333/MindBridge>

³<https://github.com/xiaoyao3302/UniBrain>

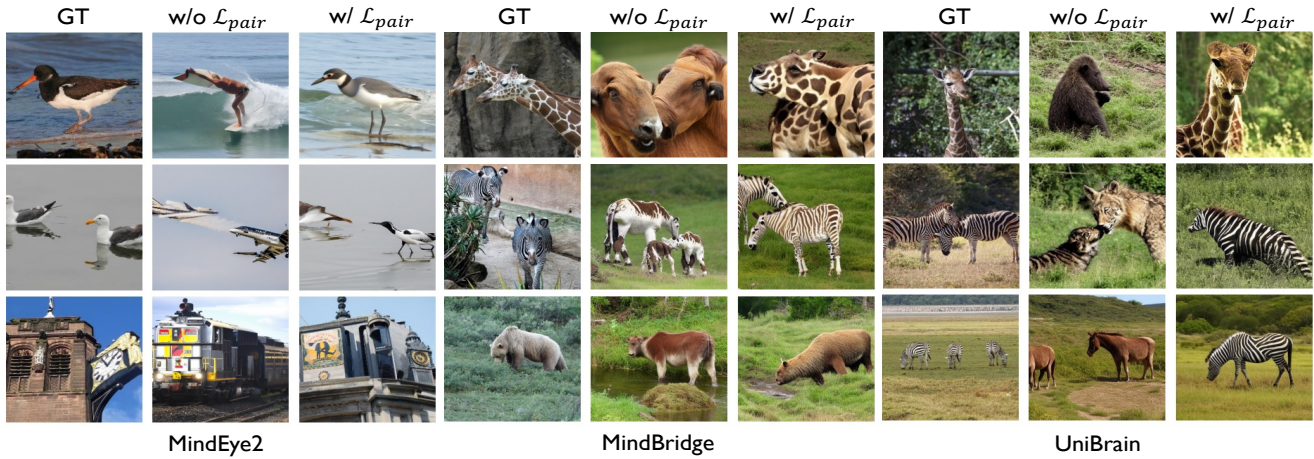


Figure 8. Qualitative results of subject 2 with reproduced models and with \mathcal{L}_{pair}

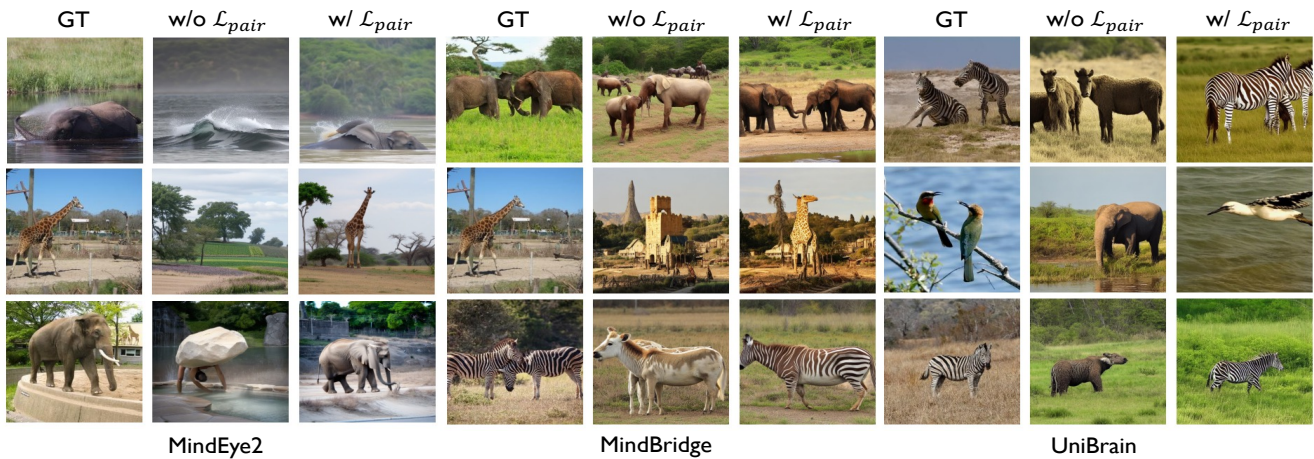


Figure 9. Qualitative results of subject 5 with reproduced models and with \mathcal{L}_{pair}

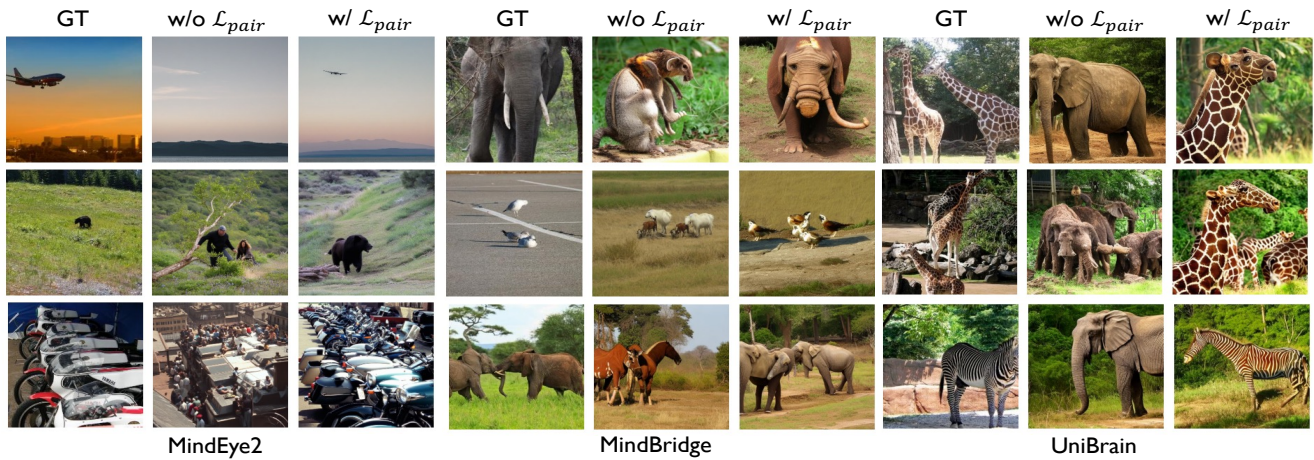


Figure 10. Qualitative results of subject 7 with reproduced models and with \mathcal{L}_{pair}

```

penalty = F.relu(-p_t_diff * t_order) # [N, N,
    N]
loss = penalty.sum() / (N * (N * (N - 1)))
return loss

```

D. Ablation Studies

D.1. Incorporation of location, size, and number information

Existence	Options			Pairwise Acc.	Kendall	Pearson
	Size	Location	Number			
✓				75.8%	.516	.708
✓	✓			75.8%	.517	.709
✓		✓		75.9%	.517	.710
✓			✓	74.7%	.493	.648

Table 4. The meta-evaluation results of Object F1 with incorporation of additional information.

We incorporate location, size, and number information into Object F1 to determine whether each factor contributes to the improvement of alignment with human judgments, as outlined below:

Size weighting We weight object categories based on their bounding box size, with larger sizes receiving higher weights. An object that fills the entire image would be weighted twice as much as an object with zero area, with scaling linearly.

Location weighting We weight object categories based on their proximity to the center of the image, with objects closer to the center receiving higher weights. An object at the center would be weighted twice as much as an object at the edge of the image, with scaling linearly.

Number count During recall and precision calculation, each object category receives partial credit if the number of detected object categories is either underestimated or overestimated, depending on the error.

The results are summarized in Tab. 4. Since none of these weighting schemes seemed to improve the metric, they were not included in the final version in order to avoid needlessly complicating the metric.

D.2. Additional results of Sec. 6.2

We present additional meta-evaluation results for all possible combinations of components of SEED in Tab. 5. Indeed, it can be observed that SEED demonstrates the best agreement with human judgments.

E. Additional Examples and Analysis of Worst-case Judgments

Here, we present additional examples of the worst-case judgments discussed in Sec. 6.4.

We report the performance of existing visual decoding models evaluated with SEED in Tab. 6.

Metric	Pairwise Acc.	Kendall	Pearson
Object F1	75.8%	.516	.708
Cap-Sim	73.8%	.477	.683
EffNet	78.0%	.559	.748
Object F1+ Cap-Sim	78.4%	.569	.774
Object F1+ EffNet	80.1%	.602	.794
Cap-Sim+ EffNet	79.2%	.583	.787
SEED	81.0%	.621	.817

Table 5. The meta-evaluation results of each metric. The best results are **bolded**.

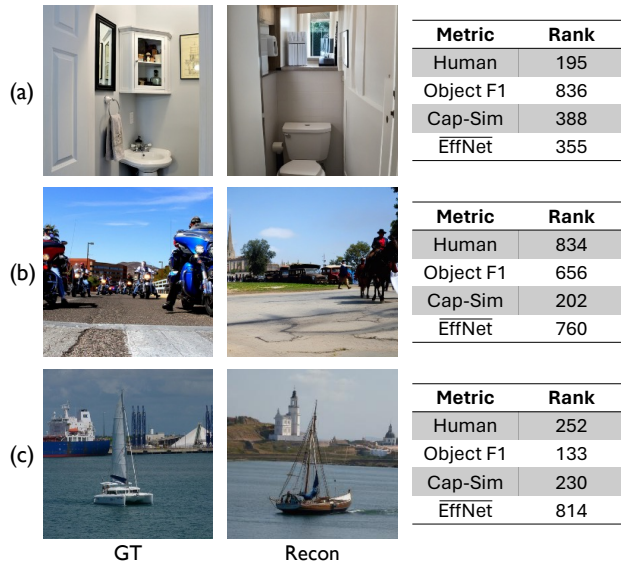


Figure 11. Additional examples of worst-case judgments

Fig. 11 (a) illustrates a case where Object F1 significantly deviates from human evaluation, assigning a score of 0. This discrepancy arises because the detected category from the GT is *Sink*, while the detected category from the reconstruction is *Toilet*. Since Object F1 evaluates similarity based solely on the presence of the detected category, it assigns a zero score, despite the reconstruction successfully generating an image that represents the concept of a restroom.

Fig. 11 (b) illustrates a case where Cap-Sim assigns a high similarity score between two images. The captions generated by GIT for the GT and the reconstruction are [A group of people riding motorcycles down a street.] and [A group of people riding horses down a dirt road.], respectively. This high similarity is likely due to the highly similar sentence structure and the Sentence Transformer’s strong emphasis on the shared action: people riding vehicles.

Fig. 11 (c) presents a case where the EffNet metric produces an extremely low correlation between two images.

Method	Low-level				High-Level				Object F1 ↑	Cap-Sim ↑	SEED ↑	SNM
	PixCorr ↑	SSIM ↑	Alex(2) ↑	Alex(5) ↑	Incep ↑	CLIP ↑	EffNet ↓	SwAV ↓				
MindEye2* [30]	.285	.380	96.0%	98.8%	95.1%	93.2%	.617	.340	.517	.548	.482	.175
NeuroPictor [11]	.228	.374	96.4%	98.4%	94.6%	93.5%	.637	.350	.481	.514	.452	.191
MindBridge [36]	.153	.285	88.4%	95.7%	92.6%	94.7%	.702	.411	.440	.483	.410	.203
UniBrain [38]	.154	.260	87.7%	95.4%	92.3%	93.7%	.695	.406	.453	.499	.419	.206

Table 6. Evaluation results with pre-trained models provided by authors. SNM represents the proportion of “semantic near-miss”. *MindEye2 was evaluated with 18 additional images, following the original work.

The ImageNet Top-1 predictions for the GT and the reconstruction are *Container ship* and *Traffic light*, respectively. This example highlights how EffNet can yield an *incorrect* evaluation due to *misclassification*.

Although the main objects in both images resemble a yacht-like boat, EffNet assigns them to different classes. We believe this occurs because the class *yacht* is not included in the 1,000 ImageNet categories. Consequently, EffNet predicts the GT as a *Container ship*, likely focusing on the ship behind the yacht, while misclassifying the reconstruction as *Traffic light*, a completely irrelevant class.

F. Re-evaluation of Existing Decoding Models

We report the evaluation results of four recent decoding models: MindEye2, NeuroPictor, MindBridge, and UniBrain. We directly evaluated the pre-trained models provided by the authors of each work. The evaluation metrics consist of eight existing evaluation metrics alongside our proposed Object F1, Cap-Sim, SEED, and the semantic near-miss rate. Note that MindEye2 was evaluated with 18 additional test image pairs as per the original work due to the sequential disclosure of the NSD dataset.